REPORT DOCUMENTATION PAGE

Form Approved
OMB No. 0704-0188

1. REPORT DATE *(DD-MM-YYYY)*	**2. REPORT TYPE**	**3. DATES COVERED** *(From - To)*
19-05-2011	Journal Article	

4. TITLE AND SUBTITLE

Ion Velocity and Plasma Potential Measurements of a Cylindrical Cusped Field Thruster

5a. CONTRACT NUMBER

5b. GRANT NUMBER

5c. PROGRAM ELEMENT NUMBER

6. AUTHOR(S)
N.A. MacDonald, C.V. Young, M.A. Cappelli, and W.A. Hargus Jr.

5d. PROJECT NUMBER

5f. WORK UNIT NUMBER
23080535

7. PERFORMING ORGANIZATION NAME(S) AND ADDRESS(ES)

Air Force Research Laboratory (AFMC)
AFRL/RZSS
1 Ara Road
Edwards AFB CA 93524-7013

8. PERFORMING ORGANIZATION REPORT NUMBER

AFRL-RZ-ED-JA-2011-172

9. SPONSORING / MONITORING AGENCY NAME(S) AND ADDRESS(ES)

Air Force Research Laboratory (AFMC)
AFRL/RZS
5 Pollux Drive
Edwards AFB CA 93524-7048

10. SPONSOR/MONITOR'S ACRONYM(S)

11. SPONSOR/MONITOR'S NUMBER(S)
AFRL-RZ-ED-JA-2011-172

12. DISTRIBUTION / AVAILABILITY STATEMENT

Approved for public release; distribution unlimited (PA #11300).

13. SUPPLEMENTARY NOTES
For publication in Journal of Physics D.

14. ABSTRACT

Measurements of the most probable time-averaged axial ion velocities and plasma potential within the acceleration channel and in the plume of a straightchanneled cylindrical cusped field thruster operating on xenon are presented. Ion velocities for the thruster are derived from laser-induced fluorescence measurements of the $5d[4]_{7/2}-6p[3]_{5/2}$ xenon ion excited state transition centered at _ = 834.72 nm. Plasma potential measurements are made using a floating emissive probe with a thoriated-tungsten filament. The thruster is operated in a power matched condition with 300 V applied anode potential for comparison to previous krypton plasma potential measurements, and a low power condition with 150 V applied anode potential. Correlations are seen between the plasma potential drop outside of the thruster and kinetic energy contours of ions with increasing velocity.

15. SUBJECT TERMS

16. SECURITY CLASSIFICATION OF:			**17. LIMITATION OF ABSTRACT**	**18. NUMBER OF PAGES**	**19a. NAME OF RESPONSIBLE PERSON**
					Dr. William A. Hargus, Jr.
a. REPORT	**b. ABSTRACT**	**c. THIS PAGE**	SAR	13	**19b. TELEPHONE NUMBER** *(include area code)*
Unclassified	**Unclassified**	**Unclassified**			N/A

Ion Velocity and Plasma Potential Measurements of a Cylindrical Cusped Field Thruster

N A MacDonald[1], C V Young[1], M A Cappelli[1] and W A Hargus, Jr.[2]

[1] Stanford Plasma Physics Laboratory, Stanford University, Stanford, CA 94305
[2] Spacecraft Propulsion Branch, Air Force Research Laboratory, Edwards AFB, CA 93524

E-mail: smacdo@stanford.edu

Abstract. Measurements of the most probable time-averaged axial ion velocities and plasma potential within the acceleration channel and in the plume of a straight-channeled cylindrical cusped field thruster operating on xenon are presented. Ion velocities for the thruster are derived from laser-induced fluorescence measurements of the $\mathbf{5}\boldsymbol{d}[\mathbf{4}]_{\mathbf{7/2}} - \mathbf{6}\boldsymbol{p}[\mathbf{3}]_{\mathbf{5/2}}$ xenon ion excited state transition centered at $\boldsymbol{\lambda} = 834.72$ nm. Plasma potential measurements are made using a floating emissive probe with a thoriated-tungsten filament. The thruster is operated in a power matched condition with 300 V applied anode potential for comparison to previous krypton plasma potential measurements, and a low power condition with 150 V applied anode potential. Correlations are seen between the plasma potential drop outside of the thruster and kinetic energy contours of ions with increasing velocity.

1. Introduction

Growing interest in the satellite community to reduce spacecraft size and cost has created a desire to scale down current plasma propulsion technologies to low power. Hall thrusters are one of the few plasma propulsion devices that have shown promise for accommodating this low power regime. However, several issues arise with Hall thrusters when scaling down in power. Studies[1, 2] on Hall thruster scaling have shown that reducing the power of a thruster by a factor of ζ requires a reduction in wall area by a factor of ζ^2. This results in increased heat flux to the discharge channel walls, especially along the center pole piece characteristic of annular Hall thrusters. Increased insulator erosion caused by this additional heat loading,[1, 2] as well as ion sputtering to the discharge chamber walls,[3] has been shown to limit the lifetime of these electric propulsion devices. The development of efficient low-power Hall thrusters is further limited by the lack of understanding of cross-field transport mechanisms which meter the flow of electrons to the anode.

Drawing from experience with Hall thrusters, several novel thruster designs have been developed in recent years to address these scaling issues. These include the so-

called cylindrical Hall thruster (CHT)[4], divergent cusped field thruster (DCFT)[5], and the cylindrical cusped field thruster (CCFT) Thruster[6]. The CHT design retracts the center pole piece that is typically a part of annular Hall thrusters, leaving a cylindrical channel[7]. This, combined with a potential drop occurring largely outside the discharge channel, reduces the impact of heat loading and erosion caused by high velocity ions impacting the channel walls.[8, 9] The CHT has demonstrated anode efficiencies ranging from $20 - 28\%$ when operating on xenon at powers between 100 and 200 W[10]. The DCFT has a conical discharge channel lined with three permanent magnets of alternating polarity. The cusped magnetic field profile diminishes in strength towards the exit plane of the thruster. The magnetic bottles between cusps mitigate electron flow directly to the anode, thereby increasing electron residence time and creating efficient ionization regions, and also minimize wall interactions due to the magnetic field pointing mostly in the axial direction. The DCFT has demonstrated anode efficiencies of around 40% in the 200 W power range.

This paper presents a study of the CCFT operating on xenon. Like the DCFT, the CCFT generates its cusped magnetic field profile by employing a series of permanent magnets of alternating polarity. The permanent magnets have varying strengths, weakening further downstream of the anode, to reproduce a similar magnetic field structure to that seen in the divergent design. However, unlike the DCFT, it has a straight cylindrical channel. Previous studies[6] have shown that when operating on krypton, the CCFT demonstrated anode efficiencies of around 23% at power levels ranging from 40 to 240 W. The discharge did not exhibit the strongly oscillating mode seen in the DCFT in high current mode[5]. While it is not yet clear how the straight configuration of the CCFT affects the discharge dynamics, we suspect that the quiescent nature to the discharge current may be attributable to the higher propellant density because of the non-divergent channel. The work presented here seeks to characterize the CCFT operating with the more commonly-used xenon propellant and employs laser-induced fluorescence (LIF) from xenon ions to study the ion transport in the very near field of the discharge. This measured ion velocity, established as a result of the kinetic acceleration of ions in the imposed electric field, is interpreted in conjunction with plasma potential measurements acquired using an emissive probe.

Time-averaged xenon ion velocities for the thruster are derived from LIF measurements of the $5d[4]_{7/2} - 6p[3]_{5/2}$ xenon ion excited state transition at $\lambda = 834.72$ nm. The measured spectral feature, which is a convolution of the ion velocity distribution function (VDF) and the transition lineshape, is used to determine the most probable axial ion velocities at various positions throughout the thruster channel and the near-field plume. These velocities (their axial components) are also used to determine the axial component to the ion's kinetic energies. Potential measurements are made using a floating emissive probe similar to that used to characterize the near-field of a low-power Hall thruster[11]. The emissive probe consists of a thoriated-tungsten thermionic electron-emitting filament, resistively heated by a direct current until saturation at the local plasma potential. The potential drop measured by the probe is then compared to

the increased kinetic energies of the ions.

2. Experiment

Figure 1 shows a schematic of the CCFT, including the magnetic field topology derived from a Finite Element Method Magnetics (FEMM) simulation of the magnetic circuit. During operation, the anode is powered at high positive potential relative to the cathode, which is at ground potential. The electric field between the anode and cathode (not shown in the figure, but located downstream and off the centerline axis) is established by the resistance imposed by the magnetic field to electron migration - a process that is not yet well understood. Propellant is introduced between the channel and the cylindrical anode at the base of the channel, upstream of a porous steel diffuser. Electrons emitted from the cathode initially migrate along the magnetic field lines gaining energy from the electric field, and colliding occasionally with propellant atoms to produce secondary electrons and avalanche ionization. The ions generated are accelerated outwards by the electric fields, and because of the relatively large ion mass, the ions are not strongly affected by the magnetic field. The electrons will mirror from regions of magnetic field convergence (cusps), and bounce between cusps increasing their residence time in the plasma, enhancing the possibility of produce electron-ion pairs through ionization. Some electrons will have enough energy to overcome sheath repulsion and will scatter off of the channel wall, allowing these electrons to "skip" across the magnetic field, eventually landing on a magnetic field line that allows it to reach either the next cusp, or the anode. The magnetic field lines also converge on the anode (graphite) located at the base of the channel centered on the channel axis. The mirroring of the electrons from this anode region provides a mechanism to restrict the electrons captured by the anode. It is anticipated that the overall performance of this thruster will depend on the location of this anode relative to the magnetic topology; however, for the studies described here, the anode location was not varied.

The construction of the thruster channel is relatively simple. The CCFT outer aluminum casing is 7 cm in length with an outer diameter of 6 cm. The cylindrical channel, lined with a boron nitride (BN) sleeve, is 4 cm in length and 1.4 cm in diameter, except for the chamfered edge at the exit plane. This divergent edge ensures that electrons traveling along field lines from the cathode will enter the discharge channel with a minimal number striking the front face of the thruster[6]. The magnetic field profile is generated by three samarium cobalt permanent magnets of alternating polarity and shaped by type 1018 steel spacers. These magnets reduce in strength as they approach the exit plane, creating a divergent magnetic field profile even though the channel is cylindrical.

The thruster is pictured operating on xenon in Fig. 1(b). The photograph in this figure is a side view, with the exit of the cathode facing the direction of observation. Apparent in this figure is a bright, luminous conical region, similar to that seen in the DCFT [5], indicating that the shape of this luminous plasma is not the divergence of

the channel, but rather, the magnetic field topology.

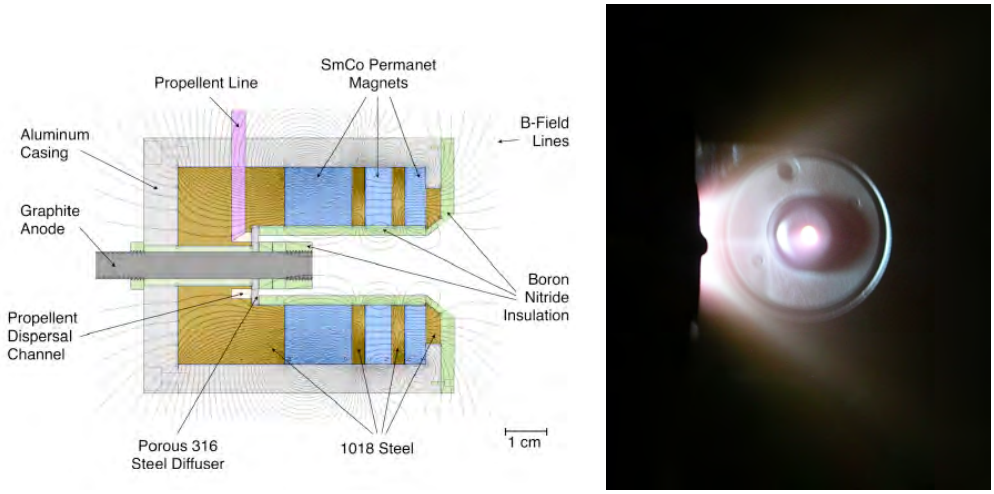

(a) DCF Schematic (b) DCF Operating on Xenon

Figure 1. (a) Schematic of DCF developed by Stanford including magnetic field simulated by FEMM. (b) DCF thruster operating on xenon propellant under power matched conditions.

Two operating conditions were examined in this study. The first was chosen to reproduce conditions seen in a previous study[6], where extensive probe measurements were taken on the CCFT running on krypton propellant at 111 W anode power. In this study the thruster was run using xenon as the propellant, with an applied anode potential of 300 V and propellant flow rate of 147 $\mu g/s$ Xe to achieve the 111 W anode power. This condition is summarized in Table 1. The second operating condition, summarized in Table 2, was chosen to highlight the low power capabilities of this thruster, with an operating power of 43.5 W. Both operating conditions were very quiescent, showing no oscillations in anode discharge current.

Table 1. Power matched operating condition.

Anode Flow	690 $\mu g/s$ Xe
Anode Potential	300 V
Anode Current	0.37 A

Table 2. Low power operating condition.

Anode Flow	690 $\mu g/s$ Xe
Anode Potential	150 V
Anode Current	0.29 A

Laser-induced fluorescence (LIF) measurements were performed at the Air Force Research Laboratory at Edwards AFB, CA. The thruster operated in a vacuum facility

capable of maintaining a background pressure of 5×10^{-6} Torr during thruster operation. A Busek cathode was used as the electron source, with specifications described in Table 3. Plasma potential measurements were performed at the Stanford Plasma Physics Laboratory (SPPL) at Stanford University. The background chamber pressure for this facility was 1×10^{-5} Torr while operating the thruster. During the tests at Stanford, an Iontech cathode was used, as a Busek cathode was unavailable. The slight differences in cathode operation appeared to have little to no effect on the overall thruster behavior (as determined by the thruster operating characteristics); the thruser proved to be invariant to changes in supplied cathode current between 0.25 to 1.3 A. Cathode position has been shown to be more critical to thruster operation, and so the cathode was placed in the same position[12] relative to the cylindrical channel for both sets of tests. The difference in background chamber pressures has been shown in previous work[13, 14] to affect ion acceleration, with higher pressures pushing the peaks in acceleration upstream towards the anode. The background chamber effects, and the inherently intrusive nature of emissive probes (as compared to the non-intrusive nature of laser diagnostics), should factor into the comparison of the LIF and plasma potential measurements made here.

Table 3. Cathode operating conditions.

Cathode	Cathode Flow	Keeper Current	Heater Current
Busek	150 $\mu g/s$ Xe	0.5 A	3.0 A
Iontech	140 $\mu g/s$ Ar	0.25 A	6.0 A

The LIF experimental apparatus at AFRL has been described extensively in previous work[15, 16]. Ion velocity measurements are accomplished by probing the $5d[4]_{7/2} - 6p[3]_{5/2}$ electronic transition of Xe II at 834.72 nm with a tunable external-cavity diode laser (New Focus, Model TLB-6017). The upper state of this transition is shared by the relatively strong $6s[2]_{3/2} - 6p[3]_{5/2}$ transition at 541.92 nm[17], allowing for non-resonant fluorescence collection. Ion velocities are determined by measuring the Doppler shifted fluorescence excitationi spectrum[18]. This particular transition has been used in past studies to characterize a variety of thrusters operating on xenon[19, 15, 14, 20].

Emissive probe plasma potential measurements in low power plasma propulsion sources have also been described extensively in previous work[6, 11]. The emitting portion of the probe consists of a 2 mm diameter loop of 150 μm diameter thoriated-tungsten (1%) wire, connected to copper wire encased in a 2.5 mm diameter alumina tube. 2.5 A of direct current is driven through the probe to heat the thoriated-tungsten filament until its signal is saturated, at which point the probe filament is floating at the potential of the surrounding plasma.

3. Results and Discussion

The ion velocities presented here represent most probable (or peak) values in an axial ion velocity distribution calculated from the Doppler shift in laser fluorescence excitation spectrum relative to the absorption peak recorded in a stationary xenon discharge reference. Contour plots of the most probable axial ion velocities are shown in Figure 2, where (a) shows the power matched condition and (b) shows the low power condition. Δ symbols indicate measurement locations. Interpolation around these points is accomplished using an inverse-distance method, given by Equation 1, where where φ_d is the velocity at the destination point and φ_s is the velocity at each source point. The weighting function, w_s, is given by Equation 2, where D is the distance between the source point and the destination point and E is a weighting factor chosen to be 3.5.

$$\varphi_d = \frac{\sum w_s \varphi_s}{\sum w_s} \tag{1}$$

$$w_s = D^{-E} \tag{2}$$

This interpolation scheme is representative of the analysis throughout these results. The white regions in the lower right hand corner of the plots represents the chamfered edge of the thruster channel, with the exit plane located at $Z = 0$ mm.

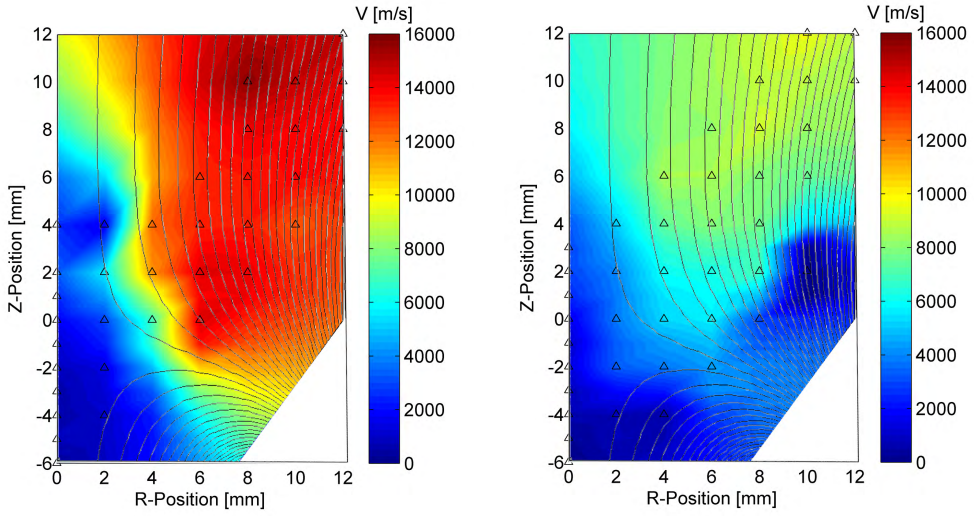

(a) Power Match (b) Low Power

Figure 2. Most probable axial ion velocities for DCF operating under (a) power matched, and (b) low power operating conditions. Δ symbols indicate measurement locations.

For the power matched condition, the ions inside the thruster channel retain a relatively low axial velocity ($\leq 2,000$ m/s) along the thruster centerline. Off axis, at radial locations greater than $R = 6$ mm, the axial ion velocities increase significantly, especially near the chamfered edge of the thruster, which contains the outermost (third)

magnetic cusp. As seen in Figure 1(a), this third magnetic cusp intersects the center of the chamfered edge, defining a separatrix which appears to form a boundary between an ionization region characterized by low ion velocity, and a region of strong axial ion acceleration. It appears therefore, that there is a close relation between the separatrix and the plasma potential. Downstream of the separatrix, the ions reach a maximum axial velocity in this region of 15,600 m/s at $Z = 10$ mm, $R = 8$ mm. In general, the ions with higher axial velocity appear away from the centerline, in the region corresponding to the visibly luminous, cone-shaped plume in Figure 1(b).

The low power operating condition shows similar trends in the contour plot of axial ion velocity, with the overall magnitudes being expectedly lower due to the lower applied anode potential (150 V vs. 300 V for the power matched condition). The lower velocity ions reside closer to the centerline inside the thruster, while higher velocity ions (reaching 9,600 m/s axial velocity) appear farther into the plume at radii > 8 mm. That the axial component of velocity peaks off-axis is even more apparent at this low power conditions, where at an axial location of z = 2 mm, the axial ion velocity peaks at a radial location of r = 4 mm. The boundary of the acceleration region does not appear to be as directly related to the separatrix near the exit plane of the thruster, indicating that the shaping of the plasma potential field by the magnetic topology depends on discharge operating conditions. We also find that the region of low axial ion velocity along the centerline does not extend as far into the plume. Rather, acceleration appears to occur at all radii across the exit plane between $Z = 2$ mm and $Z = 6$ mm. For example, the power matched condition has a peak axial ion velocity of 15,600 m/s and a maximum axial velocity of 9,400 m/s along the centerline, whereas the centerline axial velocity for the low power condition peaked at 6,500 m/s, which is more comparable in magnitude to the 9,600 m/s seen away from the centerline. When operating in the low power mode, the luminous region was distributed throughout the center of the plume instead of just the outer cone shaped region, and it was visibly less bright the power matched condition. This could be attributed, in part, to the more even distribution of ions moving throughout the cone shaped plume with lower average velocity.

Figure 3 shows the emissive probe measurements of the plasma potential, ϕ_p for both operating conditions. Probe data was taken in a horizontal plane passing through the center of the thruster exit plane and cathode, excluding area occupied by the cathode and a bolt on the exterior face of the thruster. For the power matched condition, the maximum plasma potential measured in the plume was 37 V at the edges of the discharge channel wall near the exit plane of the thruster ($Z = 0$ mm, $R = \pm 10$ mm). By 20 mm into the plume, the plasma potential drops to around 20 V, except for a conical jet of higher potential at an angle of 35° with respect to the outward normal from the exit plane which remains as high as 30 V by 20 mm into the plume. The jet is asymmetric, being interrupted on the cathode side by a region of lower potential ($\approx$ 10 V). The region of elevated plasma potential corresponds visually with the luminous conical jet seen in Figure 1(b). When operating on krypton, this region also correlated with the highest ion current density[6].

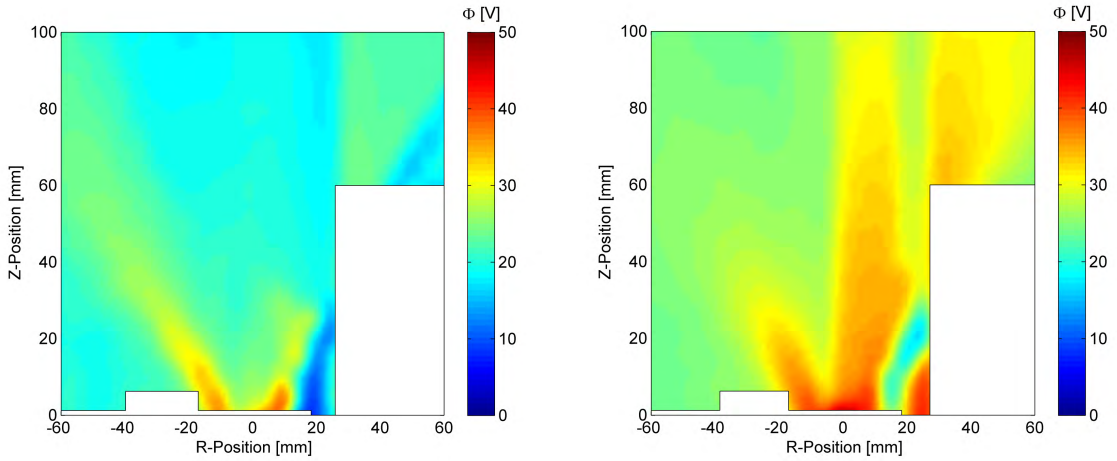

(a) Power Match (b) Low Power

Figure 3. Plasma potential measurements in the near-field DCF thruster plume operating under (a) power matched, and (b) low power operating conditions.

For the low power condition, the maximum plasma potential measured was higher than the power matched condition: 46 V at the exit plane of the thruster along the centerline ($Z = 0$ mm, $R = 0$ mm). The potential profile also displays a somewhat conical shape in the regions of higher potential; however, the potential also remains elevated throughout the center of the cone (upwards of $\approx$ 35 V on the cathode side). Once again, this corresponds to the distribution of luminous regions observed throughout the conical plume. Of note when comparing the two operating conditions, the power matched case has a larger potential drop inside the thruster channel (300 V to less than 50 V at the exit plane), whereas the low power case has a potential drop that is more distributed throughout the plume (only 150 V to $\approx$ 60 V at the exit plane). With the bulk of the plume remaining at a 25 to 35 V plasma potential, the low power condition appears to be less efficient at converting applied anode potential to ion acceleration.

Figure 4 gives a close-up of the plasma potential measurements, including points inside the discharge channel, with overlaid contours of the axial kinetic energy profiles derived from LIF measurements of axial ion velocity. Radial LIF measurements were not taken in this experiment; therefore, the kinetic energy contours should not be taken as an overall magnitude. For the power matched condition, Figure 4(a) shows that there is a large drop in potential between $Z = -6$ mm inside the thruster channel and the exit plane at radii less than $R = 7$ mm (i.e. the radius at the edge of the cylindrical portion of the thruster channel). The border between high and low potential follows a portion of the kinetic energy contour that delimits $\approx$ 20 eV ions. However, this 20 eV region extend 8 mm into the plume, while the potential drop appears contained within the thruster. The plasma potential remains relatively constant $\approx$30 V outside the thruster. This appears not to match the gradient seen in the kinetic energy contours, where ions gain energy from 20 eV to 160 eV by 12 mm into the plume.

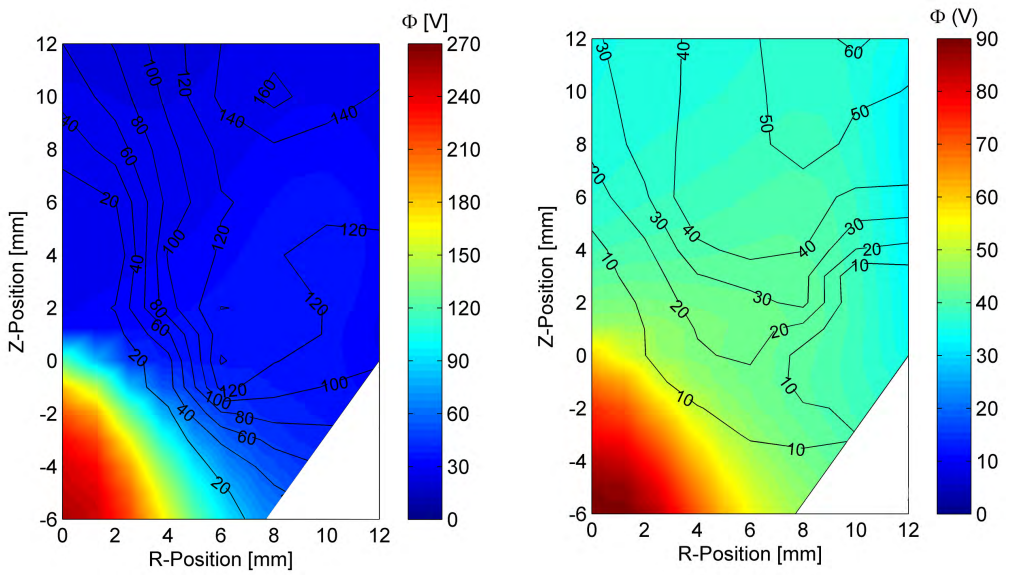

(a) Power Match (b) Low Power

Figure 4. Close up of plasma potential with kinetic energy contour overlay for the DCF thruster plume operating under (a) power matched, and (b) low power operating conditions.

Qualitatively, the low power plasma potential map seen in Figure 4(b) is very similar to the power match condition, exhibiting a large potential drop just inside the thruster exit plane followed by relatively constant potential out to 12 mm. The potential drop inside the thruster is less severe for the low power condition, only decreasing from 90 V to 40 V, compared to the 230 V drop seen in the power matched condition. Again, the lowest kinetic energy contour (this time 10 eV) more closely matches the potential drop, however the gain in axial kinetic energy outside the exit plane is unmatched by any further potential drop.

Figure 5 shows the plasma potential and ion kinetic energies along the centerline of the thruster for both the power matched and low power operating conditions. This figure better illuminates the differences between the LIF and probe measurements, as well as those between the two operating conditions. The sharp potential drop seen near the exit plane for the power match condition is more gradual for the low power case. For both conditions, the majority of the gain in axial ion kinetic energy does not occur until approximately 5 mm outside of the thruster, at which point the plasma potential has already flattened out to a nearly constant value.

The differences between the plasma potential maps and LIF derived kinetic energies could have several causes. As mentioned above, the difference in background pressure at the two facilities could slightly shift the regions of ion acceleration corresponding to the drop in potential. The SPPL chamber background pressure was approximately twice that of the AFRL chamber, likely resulting in the potential drop and peak ion acceleration being pushed upstream. Also, emissive probes are inherently intrusive by

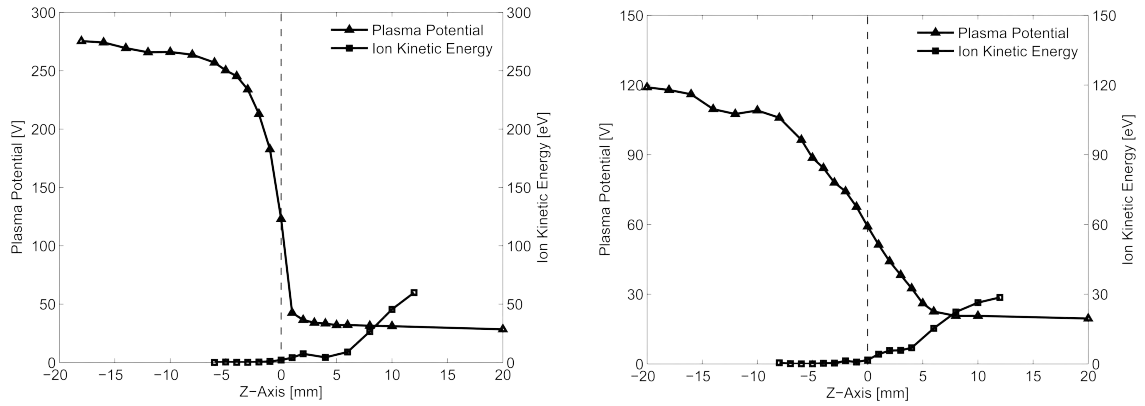

(a) Power Match (b) Low Power

Figure 5. Plasma potential and axial ion kinetic energy measurements along the centerline of the DCF thruster operating under (a) power matched, and (b) low power operating conditions.

nature, with the potential to alter the operation of the thruster, especially when taking measurements inside the thruster channel. Therefore, when comparing measurements from the different facilities, differences should be expected, especially near the exit plane of the thruster.

4. Conclusions

Laser induced fluorescence velocimetry and emissive probe plasma potential measurements were used to characterize a Stanford University developed DCF thruster operating on xenon. Two operating conditions were considered, including a condition that was power matched to a previous[6] operating condition running on krypton propellant, and a low power operating condition that had half the supplied anode potential of the power matched case. Contour plots of the most probable axial ion velocities revealed several trends: low velocity ions resided inside the thruster channel away from the walls and extended along the centerline into the plume, and a conical jet of ions had higher axial velocity outside the separatrix formed by the third magnetic cusp. Plasma potential measurements also suggested this conical profile, which was asymmetric due to the influence of the cathode for both conditions. The low power case had a higher plasma potential distributed throughout the plume than the power match condition, which mainly had high potential in the conical jet regions.

Comparisons between the plasma potential and LIF derived kinetic energies revealed that for both operating conditions, the majority of the potential drop occurred inside the thruster channel, whereas there was a significant gain in axial kinetic energy just outside the exit plane. These differences are mainly attributed to the intrusive nature of probes altering the operation of the thruster, and the higher background chamber pressure seen at SPPL causing the potential drop (and thereby acceleration region) to be moved upstream into the thruster channel. Overall, the power matched

condition appeared to more effectively convert the applied anode potential into ion kinetic energy.

Acknowledgments

The authors would like to thank A. Smith of Stanford University and B. Gregory, Lt. A. Campos, and G. Arzonia of AFRL for their technical support. N. MacDonald acknowledges the Science Mathematics and Research for Transformation (SMART) scholarship program for support of her research. C. Young acknowledges support through the Stanford Graduate Fellowship (SGF) program. Research at Stanford is funded through the Air Force Office of Scientific Research with Dr. M. Birkan as grant monitor.

References

[1] Khayms V, Martinez-Sanchez M. Design of a miniaturized Hall thruster for microsatellites. In: Proceedings of the 32nd AIAA, ASME, SAE, and ASEE, Joint Propulsion Conference and Exhibit; 1996. .

[2] Schmidt DP, Meezan NB, Jr WAH, Cappelli MA. A low-power, linear-geometry Hall plasma source with an open electron-drift. Plasma Sources Science and Technology. 2000;9:68–76.

[3] Kim V. Main Physical Features and Processes Determining the Performance of Stationary Plasma Thrusters. Journal of Propulsion and Power. 1998;14(5):736–743.

[4] Raitses Y, Fisch NJ. Parametric investigations of a nonconventional Hall thruster. Physics of Plasmas. 2001;.

[5] Courtney DG, Martinez-Sanchez M. Diverging Cusped-Field Hall Thruster (DCHT). In: Proceedings of the 30th International Electric Propulsion Conference, Florence, Italy. 39; 2007. .

[6] Young CV, Smith AW, Cappelli MA. Preliminary Characterization of a Diverging Cusped Field (DCF) Thruster. In: Proceedings of the 31st International Electric Propulsion Conference. IEPC-2009-166. American Institute of Aeronautics and Astronautics; 2009. .

[7] Raitses Y, Granstedt E, Smirnov A, Merino E, Fisch NJ. Effects of Cathode Electron Emission on Hall Thruster Discharge. In: Proceedings of the 44th AIAA/ASME/SAE/ASEE Joint Propulsion Conference & Exhibit; 2008. .

[8] Raitses Y, Smirnov A, Fisch NJ. Cylindrical Hall Thrusters. In: Proceedings of the 37th AIAA Plasmadynamics and Lasers Conference. AIAA-2006-3245. American Institute of Aeronautics and Astronautics; 2006. .

[9] Smirnov A, Raitses Y, Fisch NJ. Plasma measurements in a 100 W cylindrical Hall thruster. Journal of Applied Physics. 2004;95(5):2283–2292.

[10] Smirnov A, Raitses Y, Fisch NJ. Experimental and Theoretical Studies of Cylindrical Hall Thrusters. Physics of Plasmas. 2007;14(057106).

[11] Smith AW, Cappelli MA. Time and space-correlated plasma potential measurements in the near field of a coaxial Hall plasma discharge. Physics of Plasmas. 2009;16:073504.

[12] Young CV. Stanford University; 2010.

[13] Nakles MR, Hargus Jr WA. Background Pressure Effects on Internal and Near-field Ion Veloicty Distribution of the BHT-600 Hall Thruster;. AIAA, Preprint (2009).

[14] MacDonald NA, Cappelli MA, Hargus Jr WA. Laser-Induced Fluorescence Velocity Measurements of a Low Power Cylindrical Hall Thruster. In: Proceedings of the 31st International Electric Propulsion Conference; 2009. .

[15] Hargus Jr WA, Nakles MR. Ion Velocity Measurements within the Acceleration Channel of Low-Power Hall Thruster. IEEE Transactions on Plasma Science. 2008 October;36(5):1989–1997.

[16] Hargus Jr WA, Charles CS. Near Exit Plane Velocity Field of a 200-Watt Hall Thruster. Journal of Propulsion and Power. 2008;24(1):127–133.

[17] Hansen JE, Persson W. Revised Analysis of Singly Ionized Xenon, Xe II. Physica Scripta. 1987;(4):602–643.

[18] Demtroeder W. Laser Spectroscopy: Basic Concepts and Instrumentation. Springer-Verlag; 1996.

[19] Manzella DH. Stationary Plasma Thruster Ion Velocity Distribution. In: Proceedings of the 30th Joint Propulsion Conference and Exhibit. AIAA-1994-3141. American Institute of Aeronautics and Astronautics; 1994. .

[20] Mazouffre S, Gawron D, Kulaev V, Sadehgi N. Xe+ Ion Transport in the Crossed-Field Discharge of a 5-kW-Class Hall Effect Thruster. IEEE Transactions on Plasma Science. 2008 October;36(5):1967–1976.